Resonant steps and spatiotemporal dynamics in the damped dc-driven Frenkel-Kontorova chain

Zhigang Zheng*

*Department of Physics and Center for Nonlinear Studies, Hong Kong Baptist University, Hong Kong, China
and Department of Physics, Beijing Normal University, Beijing 100875, China*

Bambi Hu

*Department of Physics and Center for Nonlinear Studies, Hong Kong Baptist University, Hong Kong, China
and Department of Physics, University of Houston, Houston, Texas 77204*

Gang Hu

*Center of Theoretical Physics, Chinese Center of Advanced Science and Technology (World Laboratory), Beijing 8730, China
and Department of Physics, Beijing Normal University, Beijing 100875, China*

The kink dynamics of the damped Frenkel-Kontorova (discrete sine-Gordon) chain driven by a constant external force is investigated. Resonant steplike transitions of the average velocity occur due to the competition between the moving kinks and their radiated phasonlike modes. A mean-field consideration is introduced to give a precise prediction of the resonant steps. Slip-stick motion and spatiotemporal dynamics on those resonant steps are discussed. Our results can be applied to studies of the fluxon dynamics of one-dimensional Josephson-junction arrays and ladders, dislocations, tribology, and other fields. [S0163-1829(98)04833-4]

I. INTRODUCTION

Much attention has been paid in the past twenty years to simple many-body systems with an effort to disentangle the complexity of macroscopic systems with competing interactions. The well-known Frenkel-Kontorova (FK) model, which describes a chain of atoms interacting with nearest-neighboring forces and subject to a periodic substrate potential, is one of the simplest capable of capturing the essential complexities.[1-3] In dimensionless form, the Hamiltonian of the FK chain reads

$$H = \sum_{j=1}^{N} \left[\frac{1}{2} p_i^2 + V(x_j) + U(x_{j+1} - x_j) \right], \qquad (1)$$

where x_j denotes the position of the ith element in the chain and p_i is the corresponding momentum. The first term represents the kinetic energy per element. $V(x)$ describes the substrate potential, which is assumed to be a periodic form, i.e., $V(x) = V(x+b)$ with b the substrate period. $U(x_{j+1} - x_j)$ describes the interaction between the nearest-neighbor elements, which is either convex or nonconvex, depending on the studied physical systems. The formula in the Hamiltonian (1) contains both substrate interactions and mutual couplings between elements, which may lead to complicated spatially modulated structures. Spatially modulated patterns have been experimentally observed in many condensed matter physical systems, such as ferromagnetic phases of the rare earths and their compounds, long-period structures of binary alloys, graphite intercalation compounds or the polytypic phases of spinelloids, micas, perovskites and other materials.[4] In general, the physical origin of this spatially modulated behavior is the competing interactions in the free energy of systems. The FK model is one of the simplest options among many models which describe this kind of competitions. The standard FK chain can be described in terms of the following choices:

$$V(x_j) = d \left[1 - \cos\left(\frac{2\pi x_j}{b} \right) \right],$$

$$U(x_{j+1}, x_j) = \frac{1}{2} K(x_{j+1} - x_j - a)^2, \qquad (2)$$

where d, K, a, and b denote the potential barrier height, coupling strength, spring constant, and the substrate period, respectively. The commensurability of the frustration $\delta = b/a$ may strongly affect the spatial structure of the system. The ground state of the FK model has been fully investigated over the last few years, and the commensurate-incommensurate phase transitions were found and theoretically described.[3] The theory developed by Aubry[2] stands as one of the deepest achievements in theoretical comprehension of the physics of modulated phases. The responses of this system to dc (Ref. 5), ac, or both forces[6] in dissipative (inertialess) cases were also explored, where the dynamical Aubry's phase transitions and Shapiro steps (dynamical mode locking) were observed. All these studies reflect the intrinsic properties of the FK model and reveal some essential features of spatially modulated systems.

The dynamical FK model was applied to many fields, such as charge-density waves (CDW),[7] tribology and surface problems,[8] self-organized criticality (SOC),[9] and Josephson-junction arrays (JJA) (Ref. 10) and ladders (JJL).[11] Actually, the FK model is a discretized version of the sine-Gordon (SG) systems. In an experimental environment, one has to consider the effects of external influences, such as dissipations, fluctuations, and external fields, thus it is more reasonable to include all these effects. In this paper, we discuss only the spatiotemporal dynamics of a damped (inertia) stan-

dard FK chain influenced by a dc external force. It is shown[22] that the weak noise can only slightly smooth the resonances discussed below, and the influence of an ac force will induce more complicated spatiotamporal patterns. The dynamics in the dissipative (overdamped) limit under the influence of both dc and ac forces were fully discussed in relation to CDW problems and the ac effects in experiments of Josephson-junction ladder arrays,[7–11] which were found to correspond to the dynamical Aubry's phase transition and Shapiro steps, respectively. However, the inertial effects in some cases might be significant and cannot be ignored, moreover, in the underdamped region, inertial effects become dominant, multistability leads to the so-called hysteresis effects, hence the system will exhibit complicated Spatiotemporal patterns. We will focus on the underdamped case. The equation of motion discussed here can be written as

$$\ddot{x}_j + \gamma \dot{x}_j + \sin x_j = K(x_{j+1} - 2x_j + x_{j-1}) + F, \qquad (3)$$

where γ is the damping coefficient, K the coupling constant, and F the external bias. The frustration δ does not appear in Eq. (3), but it plays a significant role in the dynamics of Eq. (3). A mechanical realization is a chain of N identical damped pendula that are driven by a uniform torque and coupled by torsional springs.[12] For very large coupling and number of elements, the system (3) can be well described by the continuum SG equation. It is shown that[13] when the external applied force varies, the velocity of the SG chain has a critical value $v_c = 2\pi\delta\sqrt{K}$ that separates two kinds of dynamics (kinks). When $v < v_c$, the motion is that of localized solitons, which is called the *low-velocity regime*, and the v $-F$ relation in this regime is a continuous line. When $v > v_c$, the motion is characterized by the whirling wave, i.e., the moving kink is strongly extended, we call this regime the *high-velocity regime*. There exists an unstable region between these two regimes, which corresponds to the gap on the $v-F$ characteristics. These two regimes exist for both discrete cases and continuum cases, but the dynamics introduced by discreteness may be a distinct feature, which will not happen for the continuum cases. The whirling-instability induced resonances in the high-velocity regime were well described in Ref. 14. We will focus on the dynamics in the low-velocity regime, which is the consequence of another kind of mechanism. We shall give a precise mean-field description of resonances in this regime.

The paper is arranged as follows. In Sec. II, the dynamics in the low-velocity regime are theoretically discussed, where we will introduce a mean-field treatment which is proved to be perfectly effective.[15] This treatment results in a complete description of the resonance behavior in the low-velocity regime. Section III is devoted to numerical simulations. We show that the theory proposed in Sec. II agrees very well with numerical results by varying the mean-field parameter. In Sec. IV, the physical meaning of the mean-field consideration is discussed, which is related to Aubry's CI phase transition. Section V gives a discussion on prohibited resonances and give a resonance prohibition criterion. The high-velocity whirling mode will lead to the solitary-wave instability of some low-velocity steps. Spatiotemporal dynamics on low-velocity steps are discussed in Sec. VI. It is shown that three kinds of motions, i.e., periodic, quasiperiodic, and chaotic, can be observed on steps. We summarize the results and propose future topics in Sec. VII.

Numerical simulations will be used to study the spatiotemporal dynamics in this paper. The fourth-order Runge-Kutta integration algorithm is used and the time step is adjusted according to the numerical accuracy. Periodic boundary conditions are added, i.e., $x_{j+N}(t) = x_j(t) + 2\pi M$, where M is an integer that counts the net number of kinks trapped in the ring, therefore the frustration is $\delta = M/N$ and the spring constant will be $a = 2\pi\delta$. We mainly discuss the average velocity of the chain, which is a good candidate for studying the response of the FK chain to external forces. The averaged velocity of the chain is defined as $v = (1/N)\Sigma_{j=1}^{N}\langle\dot{x}_j\rangle$, where $\langle\ \rangle$ denotes the time average.

II. KINK-RADIATION INDUCED PHASE LOCKING: RESONANT STEPS

The key consequence introduced by the discreteness of the chain is that the solitary wave will radiate small-amplitude linear waves when it moves. The mechanism behind this behavior is the competition between the harmonic chain and the periodic substrate. Due to the discreteness of the chain, it will collide with the substrate when it moves. For the continuum SG systems, the attractors in the low-velocity regime are traveling waves. Such is also the case for the discrete version, the wave is composed of a moving kink and its radiated phonon waves in its wake. This is shown in our numerical experiments. The phenomenon of the radiation by a moving kink was discussed by Currie *et al.*,[16] Peyrard and Kruskal,[17] and other authors[18] in numerical studies, and also found in experiments on Josephson-junction arrays.[10] In some cases the kink motion and its radiated waves can become phase-locked and then lead to quantized velocity of the chain under a constant force. This occurs when the linear modes are separately excited, for if many different modes are excited simultaneously the resonance will overlap and then discrete velocity cannot be observed. It should be noted that the kink shape will strongly affect the final results, as can be seen below.

Theoretical considerations were explored by several authors,[10,14] but some drawbacks and even mistakes exist in their discussions. First, the equation of motion was directly linearized to discuss the linear waves radiated by moving kinks. One should be aware that the linearization should be used around the *moving kink*, thus the direct linearization is not correct. Second, an approximation was made of the kink directly from a 2π form. This consideration is too crude to grasp the crucial points. In fact, only in some limiting cases, for example, $M=1$ and very large N, i.e., $\delta\rightarrow 0$, is this approximation valid. For finite frustration δ, the kink apparently is not a 2π form, thus the effect of kink solution should be considered. Third, all previous discussions did not consider *subharmonic resonances*, which may be very important for finite frustration (multiple trapped kinks) cases, thus the resonance condition should include the subharmonic cases. Based on the considerations of all the above points, let us give a more precise description of quantized velocities.

Assuming the static kink solution is $\{x_j^*\}$, $j=1,\ldots,N$, when it moves along the chain and linear phonon waves are

radiated in its wake due to the discreteness, then we can linearize the equation of motion (3) around the moving kink $x_j^*(t)$ by inserting $x_j(t) = x_j^*(t) + u_j(t)$ into Eq. (3) and get

$$\ddot{u}_j + \gamma \dot{u}_j + [\cos(x_j^*)] u_j = K(u_{j+1} - 2u_j + u_{j-1}). \quad (4)$$

For sufficiently small damping γ, we can neglect the dissipative term in Eq. (4) and consider the conservative case. In fact, the dissipation effect can be compensated by external driving force. We intend to get the dispersion relation of the linear phonons. The difficulty in Eq. (4) lies in the *lattice dependence of the kink solution* x_j^*. An alternative way to overcome this difficulty is to introduce the mean-field treatment, i.e., we replace the term $\cos(x_j^*)$ by an averaged quantity

$$\beta = \frac{1}{N} \sum_{j=1}^{N} \cos(x_j^*), \quad (5)$$

where we call the parameter β a contraction factor. One should note that here β is time independent, because it only depends on the *topological structure of the static kink*. (We also find the dependence of β on the external driving F, leading to an additional contraction effect. However, the present approximation already gives a very precise prediction. This effect will be discussed elsewhere.) In fact, this parameter does describe the contraction effect of the kink solution. For $\delta \to 0$, e.g., $M = 1$ and very large N, the kink solution can be approximated by the 2π form

$$x_j^*(t) = \begin{cases} 0 & \text{for } j < vt, \\ 2\pi & \text{for } j > vt. \end{cases} \quad (6)$$

Then we immediately get $\beta = 1$ by using Eq. (5). This is the case discussed by Watanabe *et al.*, but the story does not end here. As will be shown below, the frustration plays a crucial role in the chain dynamics. Now let us insert the linear phonon mode $u_j(t) = \exp[i(\omega_l t + kpj)]$ into Eq. (4) and use Eq. (5) instead of the lattice-dependent term $\cos(x_j^*)$ to get the dispersion relation

$$\omega_l = \sqrt{\beta + 4K \sin^2\left(\frac{1}{2} kp\right)}. \quad (7)$$

The circulation frequency of the moving kink is $\omega_k = 2\pi/T = \langle v \rangle$, the resonance between these two frequencies leads to the discrete velocity of the chain. The resonance condition reads

$$m_1 \omega_k = m_2 \omega_l, \quad (8)$$

when the kink rotating frequency and its linear mode become phase locked. The geometry constraint implies that the wave number should satisfy $kp = 2\pi \delta m_1/m_2$. Then we get the resonant velocity steps

$$v(m_1, m_2) = \omega_k = \frac{m_2}{m_1} \sqrt{\beta + 4K \sin^2\left(\frac{m_1 \delta \pi}{m_2}\right)}, \quad (9)$$

where (m_1, m_2) is an integer pair that describes the resonance between kinks and linear waves and δ is the frustration. The result we obtained here considers all the points we mentioned above, which is a complete resonant velocity
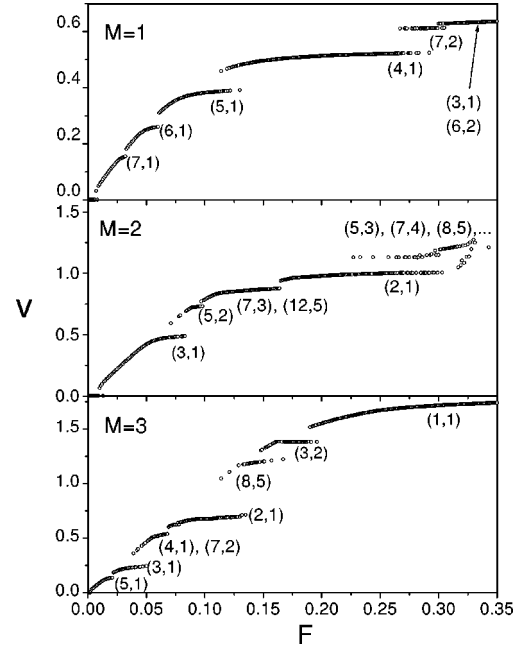

FIG. 1. The v-F characteristics for $K = 1.0$, $\gamma = 0.1$, $N = 8$, and $M = 1, 2, 3$. Resonances can be observed on the step transitions. All steps are labeled by using a pair of integers that describe the resonance between the moving localized soliton and its radiated phonons. These resonances are given by Eq. (9). The agreement is quite good. Several resonances are labeled on one step, because they are nearly degenerated.

spectrum. The significance of Eq. (9) lies in the fact that it considers the commensurability effect induced by the winding number δ, and moreover this formula relates only to the frustration δ, implying that the resonance is not a finite-size effect, but the discreteness effect. The resonance condition (8) is the main point, however, it is very strange that all authors only used the integer resonance $m_2 = 1$. In fact, one may frequently observe higher order resonant steps, as shown below. By considering both the correct resonance criterion and commensurability effect, formula (9) gives a complete description of all possible quantized velocities.

III. NUMERICAL RESULTS

We performed numerical simulations of the system (3) for different numbers of particles and other different parameters. In Fig. 1, the $v - F$ relations are given for $N = 8$, $\gamma = 0.1$ and different numbers of trapped kinks $M = 1, 2$, and 3. First we notice that all curves have resonant steps (plateaus), which are the consequences of the locking between the moving kink and its linear phonons. In many regions a given driving force corresponds to several velocities, indicating the existence of multistability. Hysteresis can be observed when one adiabatically changes the external driving force, which is a direct consequence of many attractors (metastable states). Keeping in mind that for the continuum SG system, the $v - F$ curve in low-velocity regime is a continuous line, the transition between resonant steps will result in the discontinuousness of the velocity line, replaced by many quantized values. We label the resonances on steps by a pair of integers (m_1, m_2) in terms of the theoretical formula (9); all the steps can be well predicted by using Eq. (9) if we choose $\beta = 0.55$,

TABLE I. A comparison between numerical resonant steps and theoretical predictions. All parameters are the same as those used in Fig.1. It can be clearly shown that the mean-field treatment predicts all possible resonances much better than previous predictions.

Resonance (m_1,m_2)	Numerical results	Mean-field prediction	Previous prediction
(a) $\delta=1/8$, $\beta=0.55$			
3:1	0.640	0.637	0.700
4:1	0.525	0.533	0.559
5:1	0.395	0.398	0.420
6:1	0.260	0.266	0.289
7:1	0.150	0.152	0.180
7:2	0.605	0.599	Unpredicted
(b) $\delta=2/8$, $\beta=0.25$			
2:1	1.000	1.030	1.118
3:1	0.501	0.500	0.577
5:2	0.751	0.766	Unpredicted
5:3	1.125	1.197	Unpredicted
7:3	0.850	0.855	Unpredicted
7:4	1.125	1.157	Unpredicted
8:5	1.230	1.229	Unpredicted
12:5	0.850	0.819	Unpredicted
(c) $\delta=3/8$, $\beta=0.15$			
1:1	1.800	1.888	2.100
2:1	0.720	0.733	0.866
3:1	0.250	0.286	0.420
3:2	1.368	1.333	Unpredicted
4:1	0.510	0.509	0.559
5:1	0.131	0.172	0.252
7:2	0.510	0.488	Unpredicted
8:5	1.210	1.213	Unpredicted

0.25, and 0.15 for $M=1$, 2, and 3, respectively. Subharmonic resonances can be frequently found for $M>1$, i.e., these resonances can be easily excited and locked when there is more than one kink trapped in the ring. To make a clearer comparison, Table I lists the resonances observed in Fig. 1. It can be clearly shown that Eq. (9) obtained above gives not only a much better prediction of $(m_1,1)$ resonances than previous prediction $v=(1/m_1)\sqrt{1+4K\sin^2(m_1\delta\pi)}$ (Ref. 14) but also precisely predicts high-order resonances.

Figure 2 shows several modes of motion of one of the particles in the chain for different cases. In (a), we give an evolution of a 16-particle chain with only one kink trapped inside and for a small drive. Only positive part is shown. It is observed that the velocity has a higher peak and some lower peaks. Higher peak indicates that the particle hops from one potential well to another, and the nearest lower peak is the influence of the coupling showing the hopping of the nearest-neighbor particle. Obviously the propagation of the coupling effects decays exponentially, then the chain exhibits a slip-stick motion. With increasing F, the influence of adjacent particles becomes large. (b) gives a 5:1 resonance for $N=8$ and $M=3$, where the particle hops once in each period that contains five peaks. Additionally, the multikink effect becomes evident, which is shown in (c) for a larger force. This is a high-order resonance.

One should be aware that each point on the $v-F$ curve perhaps corresponds to several attractors, not just a single attractor as pointed out by other authors. One may find both

$m_1:m_2$ and $nm_1:nm_2$ $(n>1)$ resonances at the same value of driving force when starting from different initial conditions which correspond to the same value of the average velocity. This indicates that many kinds of spatiotemporal patterns can be found. Moreover, when the resonant values are very close to each other, the velocity steps are almost degenerate and these very close modes may also interact each other to result in complicated motions.

For the weaker coupling strength K, more resonances can be excited. In Fig. 3, we give the $v-F$ plot for different couplings $K=2$, 1, 0.25, and 0.1. One finds the steps can be easily distinguished from each other for larger K. When K decreases, resonances will become vague and overlapped so that the steps cannot be well distinguished. For $K\rightarrow0$, the behavior of the chain approaches that of uncoupled particles, thus bistable solutions can be observed.[19]

An interesting problem relates to the dynamical manifestation of an incommensurate chain, for example, when the winding number δ is the golden mean $\delta_G=(\sqrt{5}-1)/2$. We mentioned that the resonant steps are only related to the winding number and independent of the number of particles. One may use the Fibonacci sequence to approach the golden mean, i.e., $\delta=\frac{5}{8}$, $\frac{8}{13}$, $\frac{13}{21}$, $\frac{21}{34}$, $\dots,\rightarrow\delta_G$. In Fig. 4, the $v-F$ characteristics are numerically calculated for the Fibonacci approach to the golden mean. Different damping parameters are adopted, but this will not affect the value of the step. This is proved in numerical computations. One can easily find the main resonant steps coincide with each other for different
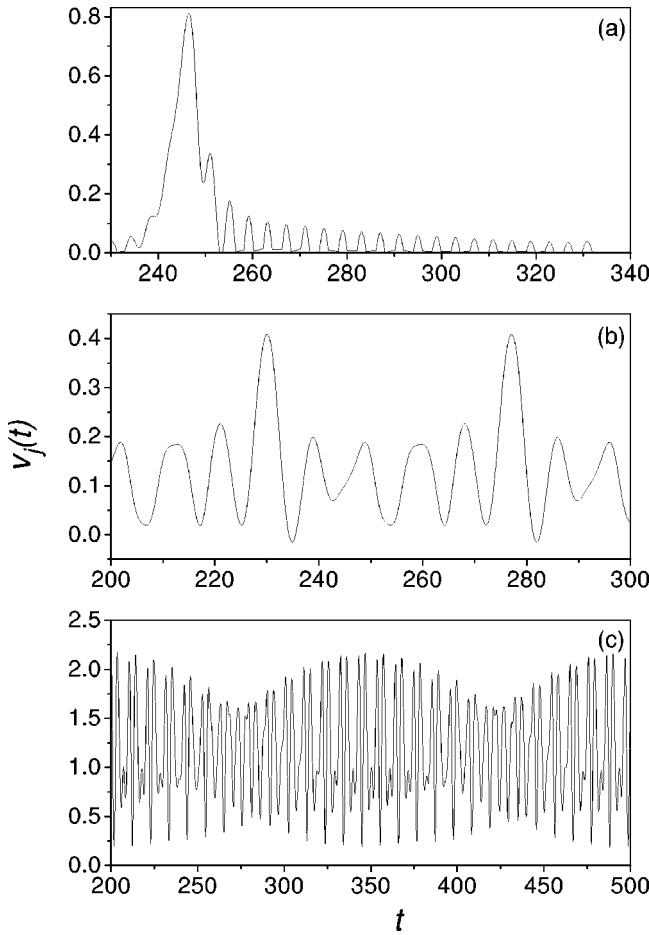
FIG. 2. The evolution of one particle in the chain for $K=1.0$, $\gamma=0.1$, and other different parameters: (a) $N=16$, $M=1$, $F=0.05$; (b) $N=8$, $M=3$, $F=0.02$; (c) $N=8$, $M=3$, $F=0.15$. Slip-stick motion can be observed in (a); high peak is the hopping from one well to another well, low peaks are the influence of neighboring-particle hoppings; the perturbation decays exponentially. (b) shows a 5:1 resonance, while (c) gives a high-order resonance.

N and M. This result proves that the resonant steps only depend on the winding number $\delta=M/N$.

IV. PHYSICAL INTERPRETATION OF THE MEAN-FIELD TREATMENT

It is shown from the above discussions that our theoretical result can precisely predict all possible resonant steps, but one may find that β varies for different frustration δ. Then a natural question arises: what is the relation between the contraction factor and the winding number? Does the contraction factor have some physical meaning? We focus on the exploration of this problem.

Because the property of β depends only on the form of the static kink, let us study the dissipative case

$$\dot{x}_j = -\cos(x_j) + K(x_{j+1} - 2x_j + x_{j-1}) + F. \qquad (10)$$

In the absence of F, Eq. (10) is used to numerically explore the ground states of the FK chain.[2] In fact, the static kink just corresponds to the ground state, which has been fully studied in recent years. Bearing this in mind, let us recall the studies
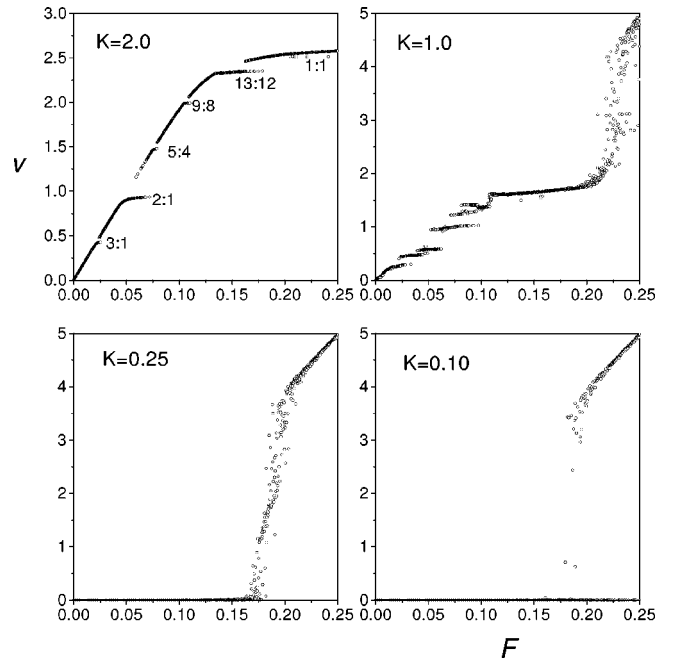

FIG. 3. The v-F relations for $N=13$, $M=8$, $\gamma=0.05$, and $K=2.0$, 1.0, 0.25, 0.1. It is shown that resonant steps can be clearly distinguished for larger coupling while the high- and low-velocity regimes will connect for weak couplings; resonances will be smoothed and disappear.

of dissipative dc-driven dynamics of the FK chain. It was found that[5] there exists a critical depinning force F_c, below which the chain will be pinned and above which the chain will slide. For a commensurate chain (rational δ), $F_c > 0$ for all K, while for the irrational δ, there exists a critical K, when $K > K_c$ the chain is pinned and when $K < K_c$ the chain slides. By averaging Eq. (10) on lattices j, one can get

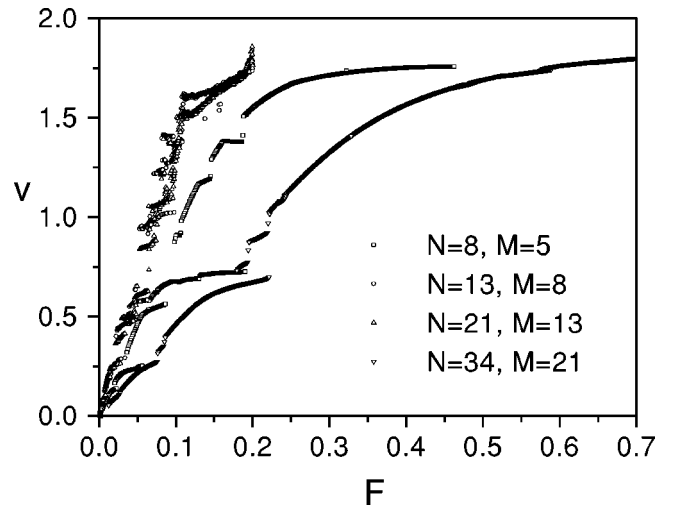$$\langle \dot{x}_j \rangle = -\langle \cos(x_j) \rangle + F. \qquad (11)$$

FIG. 4. The v-F relations for the approaching of δ to the golden mean $\delta_G = (\sqrt{5}-1)/2$ by using the Fibonacci sequence $\delta = \frac{5}{8}, \frac{8}{13}, \frac{13}{21}, \frac{21}{34}, \ldots$, for $K=1.0$ and different dampings $\gamma = 0.05, 0.1, 0.2$. Different dampings do not affect the step positions. Main steps for different cases agree well with each other.
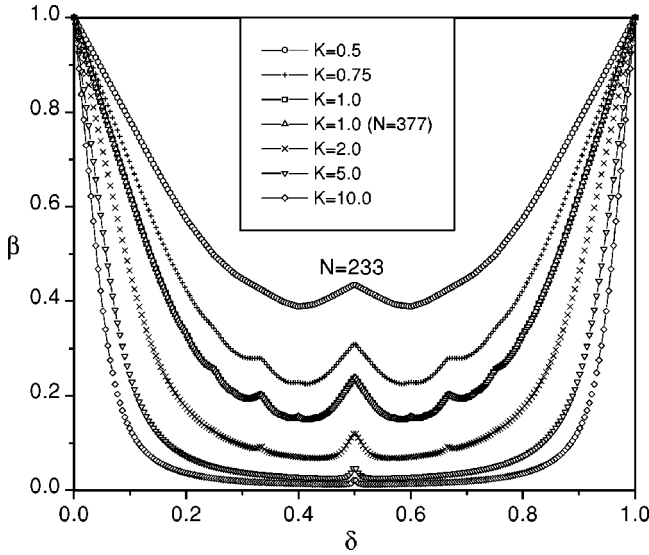
FIG. 5. The mean-field contraction factor β varying with the frustration δ. The curves are symmetric about $\delta=1/2$. The factor decreases when increasing the coupling K. Peaks are rational resonances, which form a Farey tree.

Only when $F>F_c$ can the static kink move freely along the chain, hence we readily get

$$\beta=\langle\cos(x_j^*)\rangle=F_c, \tag{12}$$

that is, β is the depinning force that is needed to overcome the Pierels-Nabarro (PN) barrier and move continuously the static kink along the chain.[2] This connection is very interesting because knowledge of Aubry's CI phase transitions now can be directly applied to this dynamical case. For example, β is directly related to the lowest phonon frequency for the FK eigenspectrum by the scaling relation $\beta\propto\omega_G^2$.

In Fig. 5, we give the relations between the contraction factor β and the frustration δ for different coupling constants. The curves are symmetric, about 0.5. This is a consequence of the symmetry of the chain. It is shown that the curves are not monotonical, i.e., many peaks can be observed. These peaks are none other than the rational resonances. The most significant resonances lie at 0:1, 1:1, and 1:2, and other resonances can also be observed for moderate K. In fact, these resonances build a Farey tree. This means all resonances can be found by using the Farey sequence $p_n/q_n, p_{n+1}/q_{n+1} \rightarrow (p_n+p_{n+1})/(q_n+q_{n+1})$. With increasing coupling K, the curve becomes lower, the contraction factor for the golden-mean winding number δ approaches 0. It is expected that there exists a critical K_c, when $K>K_c$, $\beta=0$ for δ_G. In fact, Aubry's transition from the pinned state to a sliding state occurs. In this case, the kink has the translational symmetry, thus the summation can be replaced by the integral for large N in Eq. (5), $\beta = \int_0^{2\pi}\cos(x^*)dx^*=0$. In the previous section, the values of β we chose to predict resonant steps agree very well with the $\beta-\delta$ line for $K=1.0$. It is interesting that a similar plot between the depinning force and the frustration was obtained numerically and experimentally by Ustinov *et al.*[10] for explorations of the fluxon dynamics in the Josephson-junction arrays, where the frustration corresponds to the magnetic field. This also confirms our conclusion.
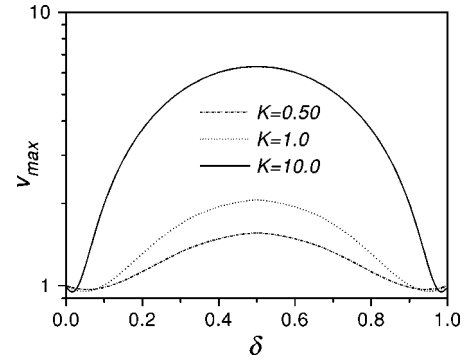

FIG. 6. The maximum velocity $v_{\max}$ varies with the frustration δ for the coupling strength $K=0.5$, 1.0, and 10.0. The effect of the contraction factor cannot be ignored for smaller K. Nonlinear regions can also be observed at the edges of the curves.

The maximum velocity occurs on the 1:1 resonant step, i.e.,

$$v_{\max}(\delta,K)=\sqrt{\beta(\delta,K)+4K\sin^2(\delta\pi)}, \tag{13}$$

which is a function of δ and K. Because the contraction factor β is a highly nonlinear function of the frustration δ, the relation between the maximum velocity and the frustration is also complicated. In Fig. 6 we give the relations $v_{\max}-\delta$ for different coupling strengths K. It can be found that the relation is rather complicated for small K, where the contraction factor cannot be neglected, while for stronger couplings, the dominant factor is the sinusoidal term, where the relation is approximately sinusoidal, $v_{\max}\propto\sin\delta\pi$. However, at the edges of all the curves, the relations are nonlinear, where β plays a dominant role.

V. RESONANCE PROHIBITION CRITERION

The agreement between theoretical and numerical results is quite good, as found from the above discussions. One may also find that not all the resonances can be observed from the numerical curves, i.e., the resonances are incomplete. Several reasons can lead to the disappearance of some steps. First, the dissipative effect should be taken into account. Large damping γ can smooth those weaker resonances. Second, the coupling strength also plays a role in the disappearance of some weaker resonances. This can be easily understood from the SG dynamics. For stronger couplings, the discreteness of the chain becomes weak. However, the above two effects are all parametric, i.e., whether the steps can be observed strongly depends on the parameter region one chooses. In fact, a third reason, an intrinsic reason, should not be ignored. That is, kink-radiation induced resonances can only occur in the low-velocity regime. Therefore a criterion should be

$$v(m_1,m_2)\leq v_c=2\pi\delta\sqrt{K}, \tag{14}$$

which means that the anticipated steps that exceeds v_c will not be observed, where v_c is the boundary between the low- and high-velocity regimes, which is pointed out in Sec. I. By inserting Eq. (9) into Eq. (14) and setting $X=m_1\delta\pi/m_2$, where $X\in[\delta\pi,\infty)$ (because $m_2\leq m_1$), we obtain the form
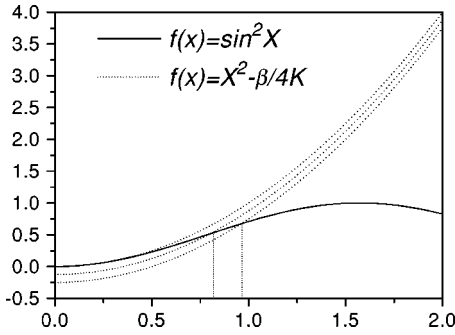
FIG. 7. Plot of the two functions $f(x) = \sin^2 x$ and $f(x) = x^2 - \beta/4K$ for $K = 1.0$ and $\beta = 1.0, 0.5$, and 0.0 (dotted lines from below).

$$X^2 - \frac{\beta}{4K} \geq \sin^2 X \quad \text{and} \quad X \in [\delta\pi, \infty). \qquad (15)$$

In Fig. 7 we plot the two functions $f(x) = X^2 - \beta/4K$ and $\sin^2 X$ for $\beta = 1, 0.5$, and 0 (dotted lines from lower to upper), respectively. For $\beta = 0$, the point of intersection of the two curves is 0, above which the inequality satisfies automatically. In this case, all possible resonances can be found. $\beta = 1$ occurs for $\delta \to 0$ or 1, where the intersection point is approximately $X_0 = 0.95$. In numerical simulations, we use usually a finite number of particles, thus the frustration is really small when M is very small and N is very large. For example, in the case $\delta = 1/N$, there are some disappeared main steps ($m_2 = 1$). The disappeared steps satisfy $m_1 \delta\pi = m_1\pi/N \leq X_0$, which leads to $m_1 \leq NX_0/\pi \approx 0.95N/\pi$. For $N = 8$, $m_1 < 3$, which is in good agreement with the observation of Fig. 1. In Fig. 8, we give the numerical $v - F$ characteristics for $N = 16$, $M = 1$. Both low- and high-velocity regimes are shown. The steps above the dotted horizontal line are whirling-mode-instability induced resonances,
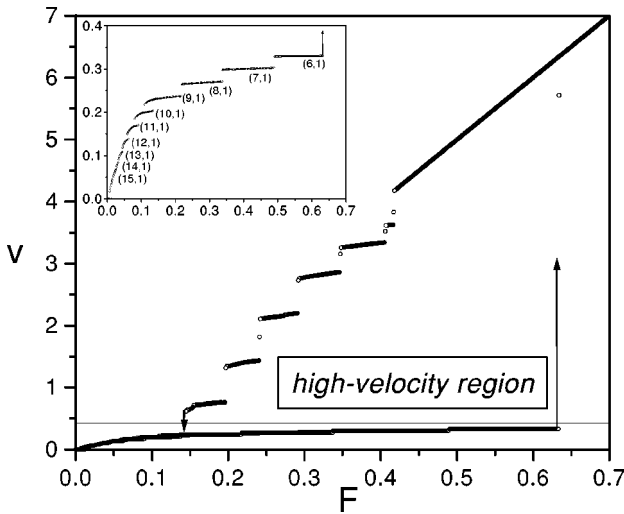
whose mechanism is different from resonances found in low regimes. Arrows show the jumps between the low and high regimes. The inset of Fig. 8 is an enlarged plot of steps in the low-velocity regime. One may find that resonances start only from 6:1. Resonances $m_1 : 1$ satisfying $m_1 < 6$ may immerse in the high regime, which become unstable due to the whirling modes. By using our criterion (15), we get $m_1 \leqslant 5$. This is the same as the numerical result in Fig. 8.

The critical frustration that indicates the disappearance of resonant steps can be determined by

$$v_{\max} = v_c = 2\pi\delta\sqrt{K}. \qquad (16)$$

When $v_{\max} < v_c$, all steps can be observed. When the frustration δ is less than a critical δ_c, $v_{\max} > v_c$, some steps begin to immerse into the high-velocity regime and cannot be observed. The critical frustration cannot be theoretically worked out from Eq. (16). We can only obtain it from the numerical computations. For $K = 0.5$, 1.0, and 10.0, we obtain $\delta_c = 0.30$, 0.222, and 0.1010, respectively.

VI. DYNAMICS ON THE STEPS

The attractors on steps are deformed traveling waves, and the phase-locking between the kink motion and the linear waves leads to resonant steps. This basic mechanism is quite simple, but the spatiotemporal dynamics on steps may be sophisticated. Dynamics on high wave number (large m_1) is a bit simple, because they can be easily excited by a small external force. For larger forces, many linear modes can be excited and they can also interact with each other, thus the dynamics become complicated. A quite interesting problem relates to the dynamics of the transitions between resonant steps. In numerical simulations, we observed three routes of motions along a step when one adiabatically increases the driving force F: Route (1): periodic→periodic→transition to new steps; Route (2): periodic→quasiperiodic→transition to new steps; Route (3): periodic→quasiperiodic→chaotic →transition to new steps.

Route (1) mainly occurs for small F cases. In this case, on a resonant step, a moving kink couples to its linear waves and they are phase locked. Further increase of the driving force will not further increase the velocity of the chain, the increase of energy is used to *amplify the linear waves*, then at a critical force the large linear wave may cause the resonance to become unstable and the transition to another step occurs. Here the coupling to linear waves can be considered as an *additional damping*. When the external drive becomes larger, several linear modes will interact with each other, leading to the quasiperiodic or even chaotic motions. The role of the drive in these cases will be both amplifying the linear waves and *exciting new linear modes*. In Fig. 9, we calculated Poincaré sections $\sin x_1 - \sin x_2$ by strobing the phases whenever the mean phase $\bar{x}(t) = (1/N)\Sigma_{j=1}^{N} x_j(t) = 0 \pmod{2\pi}$ for $N = 8$, $M = 2$ on the 7:3 step. From (a)–(e), $F = 0.112$, 0.12, 0.13, 0.15, 0.16, and 0.165, respectively. For a smaller F, the chain exhibits periodic motions, the section only contains a point; this is not shown in Fig. 9. For $F > 0.11$, the motion becomes quasiperiodic, corresponding to the emerge of a small closed torus in (a). Further increases of external force cause the quasiperiodic motion to become more complicated, the closed curve becomes *deformed*,
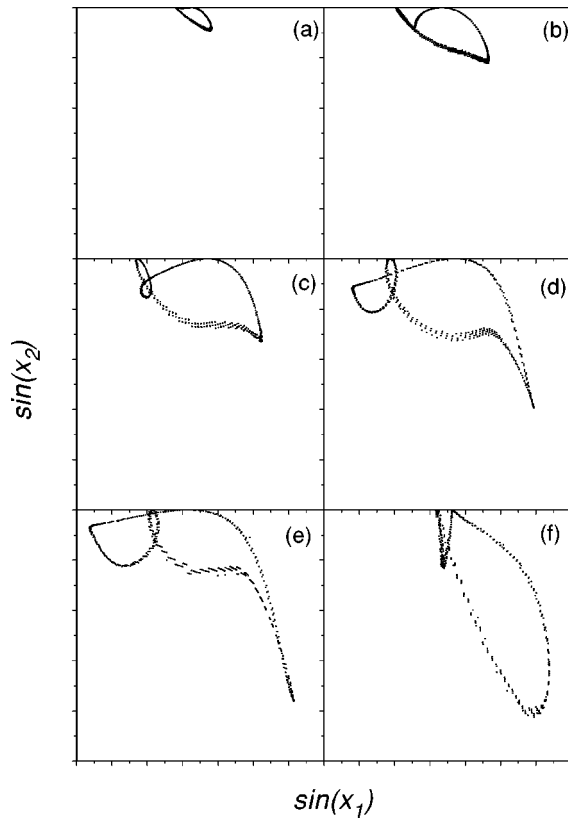

FIG. 8. The v-F plot for $N = 16$ and $M = 1$, where $K = 1.0$, $\gamma = 0.1$. Both low- and high-velocity regimes are shown. Resonances also occur in the high regime due to the whirling-mode induced parametric instability. The inset shows the enlarged plot of the low-velocity regime. All resonances are labeled by using the theoretical equation (9). Resonances $(m_1, 1)$ where $m_1 < 6$ disappear due to the resonance prohibition criterion given by Eq. (13).

FIG. 9. A historic plot of the surface of section $\sin x_2 - \sin x_1$ where the mean phase $x_-(t) = (1/N)\Sigma_{j=1}^N x_j(t) = 0 \pmod{2\pi}$ for $N = 8$, $M = 2$ on the 7:3 step. $F = 0.112$, 0.12, 0.13, 0.15, 0.16, and 0.165 for sections (a) to (e), respectively. The torus represents quasiperiodic motion. The size of the torus increases and deforms with increasing F until it breaks into a new point that denotes a periodic motion, indicating the transition to another dynamical state.

FIG. 10. An illustration of Poincaré sections $\sin x_2 - \sin x_1$ for $N = 8$, $M = 3$ on the 3:2 step, where F varies from 0.162 to 0.213 for the pictures from (a) to (l). It vividly demonstrates the bifurcation from periodic motion to qausiperiodic and chaotic motions. When F increases, the torus becomes larger and twists, then forms a web and eventually becomes chaotic.

twisted, and enlarged, indicating that the energy provided by the external drive is consumed for both exciting new linear phonons and amplifying linear waves. When F exceeds a critical value, the torus breaks, a new periodic motion emerges again, and then a new resonance occurs, which corresponds to the transition to a new resonant step. We also show a route to chaos in Fig. 10 for $N = 8$ and $M = 3$ on the 3:2 step, where F varies from 0.162 to 0.213 for the plots from (a) to (l). This image vividly demonstrates the route from the periodic to chaotic motions. We still did not plot the periodic motion, for it is only a point on the section. Then the point grows and becomes a torus, indicating the presence of quasiperiodic motion. The torus becomes larger and twists, as though in the presence of a ''saddle'' point (it is not really a saddle point), then more saddles occur in (g) and the torus becomes a ''web.'' Further increasing F leads to irregular motion. The motions in (k) and (l) become chaotic. In fact, one may study the interaction of linear modes on these steps. This problem is now under further study.

VII. CONCLUSIONS

This paper dealt with the discreteness effect of the SG chain in the low-velocity regime. Small linear phonons can be radiated when the localized kink moves along the chain in this region. When the velocity of the moving kink and its
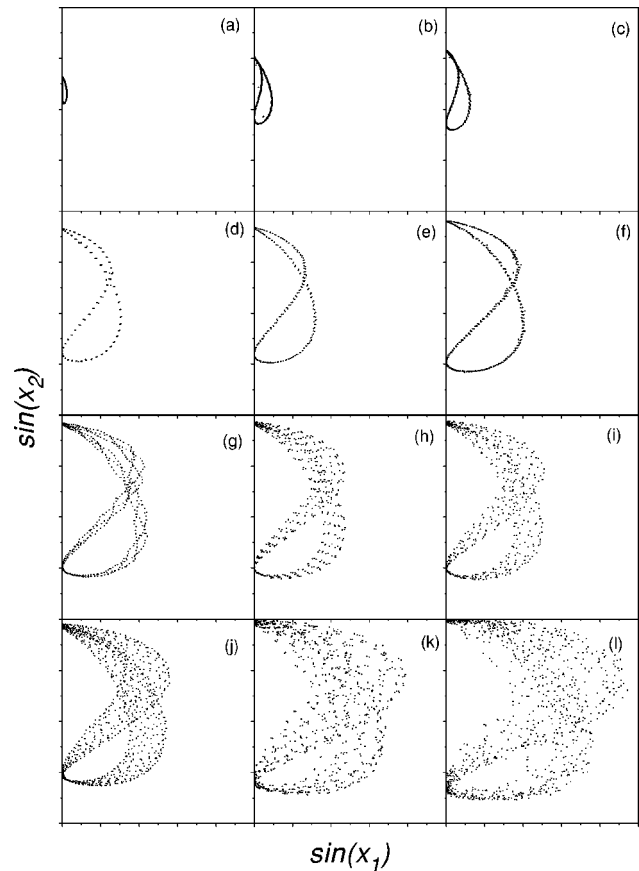
linear-wave frequency satisfy the resonance condition, the motion will be phase locked and then one can observe the resonant steps in the $v - F$ plot. We gave a mean-field treatment of the resonances and a complete description of resonant steps. Our theoretical formula can precisely predict all the steps observed in numerical simulations. In fact, we showed that the mean-field approximation is physically reasonable and that the contraction factor correponds to the depinning force that is necessary to overcome the PN barrier and freely move the static kink along the chain. This directly connects the present results to Aubry's CI phase transitions. Commensurability plays a crucial role in the kink dynamics of the discrete FK chain. Due to the gap between the low- and high-velocity regimes, in some cases not all steps can be observed. Some steps of them are prohibited to occur because they immerse into the high-velocity regime and become unstable. We derived a step prohibition criterion, which agrees very well with numerical observations. We also carefully investigated the dynamics on steps and found three kinds of dynamics of the transitions between the resonant steps. Dynamics on low steps is generally simple, only a single linear mode will participate in the competition, thus the motion is periodic. On higher steps, several linear modes can be simultaneously excited and they compete and interact, leading to quasiperiodic and chaotic motions. Every jump

from one step to a higher step can only produce periodic motion and when further increasing the drive force the linear wave is amplified and other modes are also excited, leading to complicated spatiotemporal patterns.

The damped dynamics of the FK model can be found in many fields of physics, for example in CDW, coupled damped pendula, JJL, and JJA. Special emphasis has been placed on experimental studies of fluxon dynamics in JJA and JJL in recent years. The Josephson junction is an excellent candidate for the study of nonlinear dynamics and it has been applied in many fields. Resonant steps were also observed in experiments of the current-voltage characteristics for JJL and JJA. Therefore we expect the present results can also be applied to experiments on JJA and JJL. For the JJL, the coupling mechanism is very complicated, as the coupling is usually a sinusoidal form, thus our results can only be applied to experiments of JJL for larger coupling.[22]

The noise effect on the resonant steps can cause anomalous diffusion of the Brownian motions of the damped FK chain.[20] This is quite different than the diffusion of an uncoupled group of Brownian particles in biased periodic potentials.[19,21] Another problem relates to the ac dynamics of the damped FK model. Because of competitions of many time scales, the dynamics may be complicated. This problem is currently being studied.

*Electronic address: zgzheng@public2.bta.net.cn.

[1] J. Frenkel and T. Kontorova, Phys. Z. Sowjetunion **13**, 1 (1938).

[2] S. Aubry, Phys. Rep. **103**, 12 (1984); M. Peyrard and S. Aubry, J. Phys. C **16**, 1593 (1983).

[3] W. Selke, Phys. Rep. **170**, 213 (1988).

[4] J. M. Yeomans, in *Solid State Physics* edited by H. Ehrenreich and D. Turnbull (Academic, New York, 1988), Vol. 41.

[5] S. Coppersmith, Phys. Rev. B **30**, 410 (1984); S. Coppersmith and D. Fisher, Phys. Rev. A **38**, 6338 (1988); L. Sneddon and K. Cox, Phys. Rev. Lett. **58**, 1903 (1987); L. Sneddon and S. Liu, Phys. Rev. B **43**, 5798 (1991).

[6] L. Floria and F. Falo, Phys. Rev. Lett. **68**, 2713 (1992); F. Falo, L. Floria, P. Martinez, and J. Mazo, Phys. Rev. B **48**, 7434 (1993); J. Mazo, F. Falo, and L. Floria, *ibid.* **52**, 6451 (1995); for recent reviews on dissipative dc and ac dynamics in the FK model, see L. Floria, and J. Mazo, Adv. Phys. **45**, 505 (1996).

[7] A. A. Middleton and D. S. Fisher, Phys. Rev. Lett. **66**, 92 (1991); A. A. Middleton, *ibid.* **68**, 670 (1992); A. A. Middleton, O. Biham, P. B. Littlewood, and P. Sibani, *ibid.* **68**, 1586 (1992).

[8] B. N. J. Persson, Phys. Rev. Lett. **71**, 1212 (1993); J. Chem. Phys. **103**, 3849 (1995); T. N. Krupenkin and P. L. Taylor, Phys. Rev. B **52**, 6400 (1995); E. Granato, M. R. Baldan, and S. C. Ying, cond-mat/9510058, 1995 (unpublished); M. Weiss and F. J. Elmer, Phys. Rev. B **53**, 7539 (1996); cond-mat/9704110, 1997 (unpublished).

[9] F. J. Elmer, Phys. Rev. E **50**, 4470 (1994); Helv. Phys. Acta **66**, 99 (1993).

[10] H. Zant, T. Orlando, S. Watanabe, and S. Strogatz, Phys. Rev. Lett. **74**, 174 (1995); A. Ustinov, M. Cirillo, and B. Malomed, Phys. Rev. B **47**, 8357 (1993); **51**, 3081 (1995).

[11] S. Ryu, W. Yu, and D. Stroud, Phys. Rev. E **53**, 2190 (1996); B. Kim, S. Kim, and S. Lee Phys. Rev. B **51**, 8462 (1995); J. Kim, W. Choe, S. Kim, and H. Lee, *ibid.* **49**, 459 (1994).

[12] R. A. Guyer and M. D. Miller, Phys. Rev. A **17**, 1205 (1978); **17**, 1774 (1978).

[13] Y. Kivshar and B. Malomed, Rev. Mod. Phys. **61**, 763 (1989).

[14] S. Watanabe, H. Zant, S. Strogatz, and T. Orlando, Physica D **97**, 429 (1996); S. Watanabe, S. Strogatz, H. Zant, and T. Orlando, Phys. Rev. Lett. **74**, 379 (1995).

[15] Zhigang Zheng, Bambi Hu, and Gang Hu (unpublished).

[16] J. Currie, S. Trullinger, A. Bishop, and J. Krumhansi, Phys. Rev. B **15**, 5567 (1977).

[17] M. Peyrard and M. Kruskal Physica D **14**, 88 (1984).

[18] R. Boesch, C. R. Willis, and M. El-Batanouny Phys. Rev. B **40**, 2284 (1989).

[19] H. Risken, *The Fokker-Planck Equation, Methods of Solution and Applications* (Springer-Verlag, Heidelberg, 1984).

[20] Zhigang Zheng, Bambi Hu, and Gang Hu (unpublished).

[21] Zhigang Zheng and Gang Hu, Phys. Rev. E **52**, 109 (1995).

[22] Zhigang Zheng, Bambi Hu, and Gang Hu, Phys. Rev. E **57**, 1139 (1998).